Supporting Information

Space Charge and Active-Layer Capacitance in Bulk Heterojunction Based Phototransistors

Meihua Shou,*[ab] Qinglei Zhang,[b] Yu Zhang,[b] Xuehua Hou,[b] Jiaxin Zheng,[b] Jiadong Zhou,[b] Shicheng Xiong,[b] Nan Zheng,[b] Zengqi Xie [b] and Linlin Liu*[b]

[a] Guangxi Key Laboratory of Precision Navigation Technology and Application, Guilin University of Electronic Technology, Guilin 541004

[b] Institute of Polymer Optoelectronic Materials and Devices, Key Laboratory of Luminescence from Molecular Aggregates of Guangdong Province, State Key Laboratory of Luminescent Materials and Devices, South China University of Technology, Guangzhou 510640, P. R. China

E-mail: mhshou@guet.edu.cn (M. Shou), msliull@scut.edu.cn (L. Liu)

1. The morphology of BHJ films in OPTs

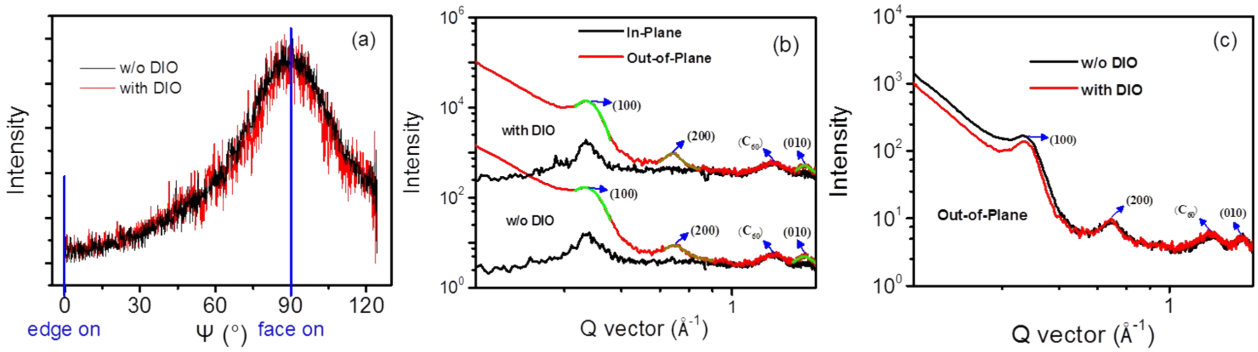

Fig. S1 (a) Pole figures of the (010) π-π stacking of crystals in the blend film with and without (w/o) DIO. (b) one-dimensional scattering profiles of in-plane and out-of-plane for PDPPBTT:$PC_{61}BM$ (1:1) blended films with DIO and w/o DIO, (c) one-dimensional scattering profiles of out-of-plane for PDPPBTT:$PC_{61}BM$ (1:1) blended films with DIO and w/o DIO.

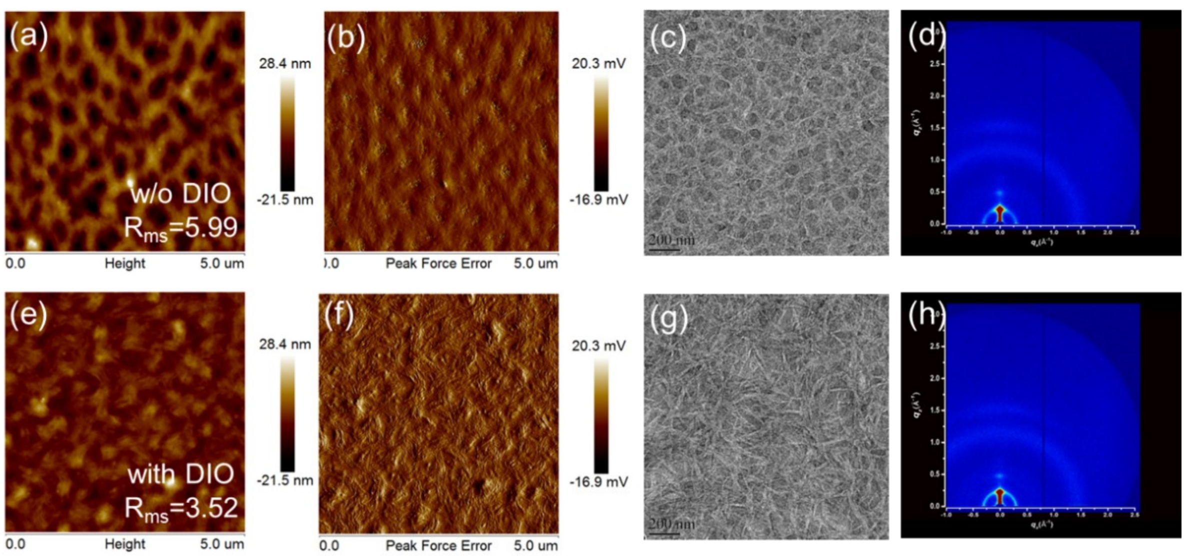

Fig. S2 AFM phase and topography images, TEM pictures and 2D GIWAXS patterns of OPTs (D/A: 1:1) w/o DIO (a-d) and with DIO (e-h), the corresponding roughness values are given in the AFM phase images.

Table S1. Center and FWHM values of diffraction peak in 1D GIWAXS profiles of OPTs (D/A: 1:1)

	crystal coherence length (100)			π-π stacking (010)		
	Q (Å-1)	Δq (FWHM)	d (nm)	Q (Å-1)	Δq (FWHM)	d (Å)
w/o DIO	0.292	0.122	4.584	1.847	0.345	3.402
with DIO	0.298	0.093	6.013	1.825	0.254	3.443

To understand the role of the solvent additive DIO, the morphology of BHJ films w/o and with DIO additive was investigated and compared using atomic force microscope (AFM), transmission electron microscopy (TEM, the darker domains correspond to $PC_{61}BM$ rich phase, the brighter parts correspond to polymer rich domains) and grazing incident wide-angle X-ray diffraction (GIWAXS, Fig. S1 and Fig. S2). The phase morphology demonstrate that the PDPPBTT:$PC_{61}BM$ blend films with DIO have much smaller domain sizes and more significant phase separation than that blend films w/o DIO, suggesting an increased D/A interfacial area and allowing for increased charge separation/recombination; besides, DIO created elongated nanofibrous continuous interpenetrating networks films through the promotion of the demixing of PDPPBTT and $PC_{61}BM$, which was essential for the exciton separation.

The above mentioned detailed morphological characterization revealed the working mechanism of solvent additive in OPT. Although the solvent additive has the same effect on the morphology of BHJ films in vertical and lateral structure, which increasing a D/A interfacial area and creating a interpenetrating network formed by small fibril like structures, the interpenetrating network formed by small fibril like structures in lateral devices is not continuous and the make of carrier transmission is different from vertical devices since the large transmission distance in lateral devices (40 μm, much larger than ~100 nm of vertical devices).

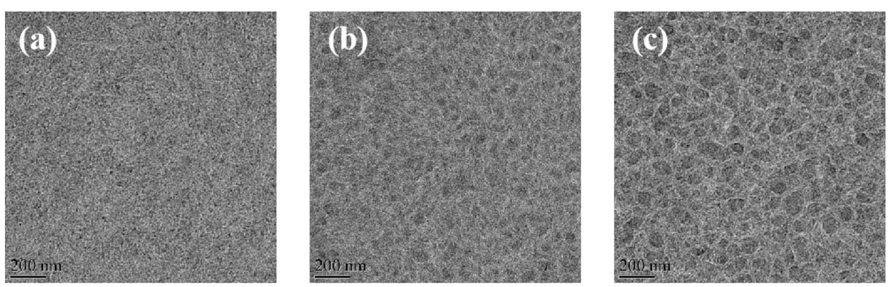

Fig. S3 TEM pictures of (a)DEVICE 5:1, (b) DEVICE 2:1, (c)DEVICE 1:1.

2. Device structure, molecular structure and energy level diagram of the OPTs

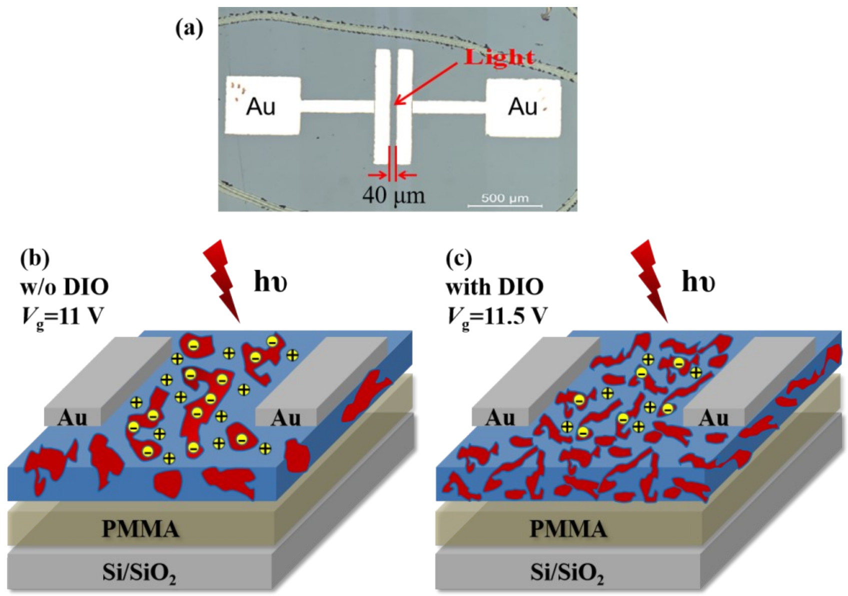

Fig. S4 (a) Top view of the device and (b,c) the schematic diagram of the device with and without DIO.

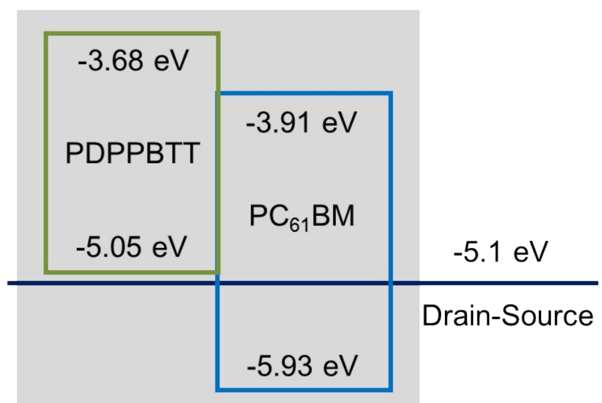

Fig. S5 Energy levels diagram of OPTs.

3. Absorption spectra

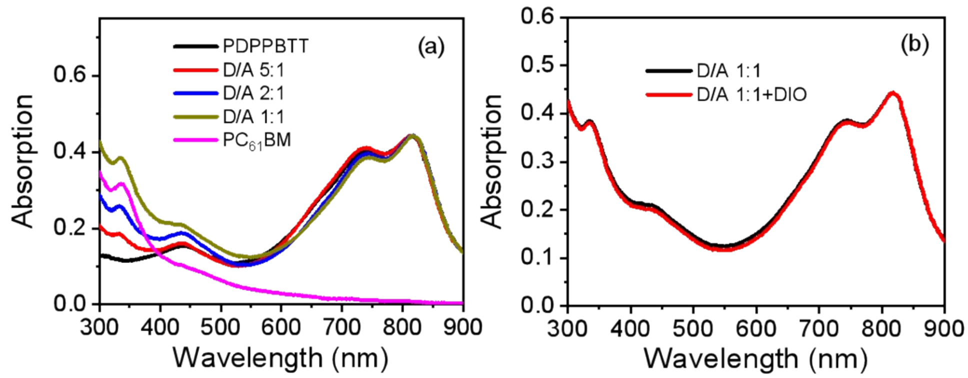

Fig. S6 Optical absorption of PDPPBTT, $PC_{61}BM$ and the blended film (a), and with/without DIO (b), which the measured structure is quartz/PMMA (45 nm)/PDPPBTT:$PC_{61}BM$ (D/A 5:1, 2:1 and 1:1).

4. Carrier lifetime of OPTs

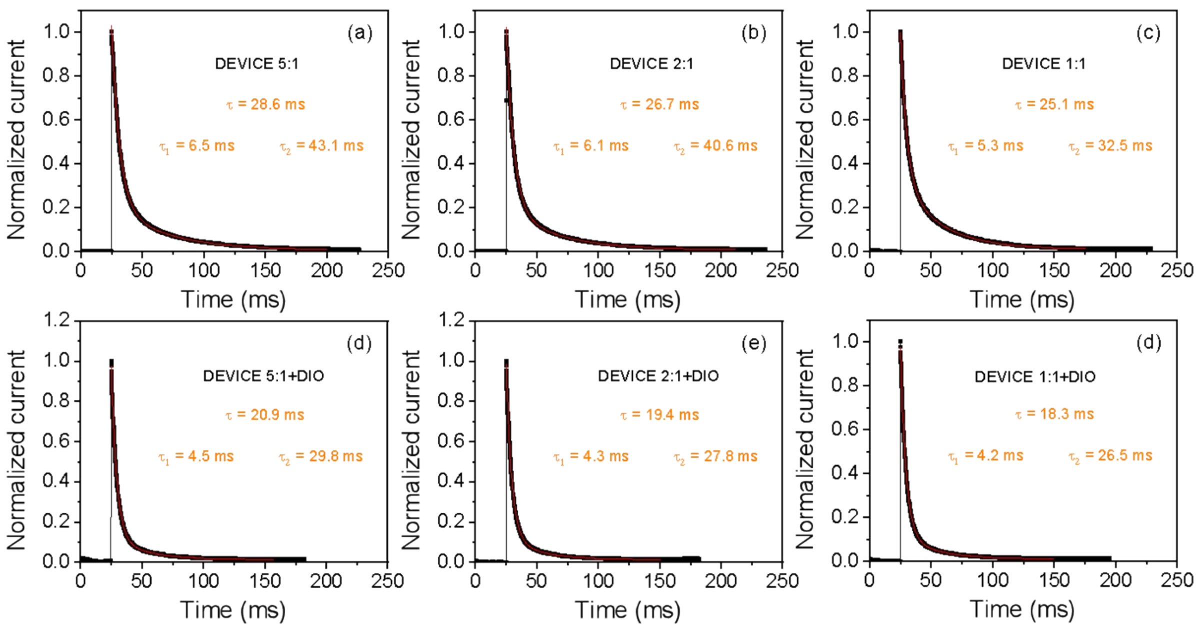

Fig. S7 Photoinduced current release characteristic curve of OPTs under 0.031 mW cm^{-2} of 820 nm pulsed excitation: (a) DEVICE 5:1, (b) DEVICE 2:1, (c) DEVICE 1:1, (d) DEVICE 5:1+3% DIO, (e) DEVICE 2:1+3% DIO and (f) DEVICE 1:1+3% DIO. The red lines are the fitting curves using exponential decay.

5. Optical responsiveness and output characteristics of OPTs

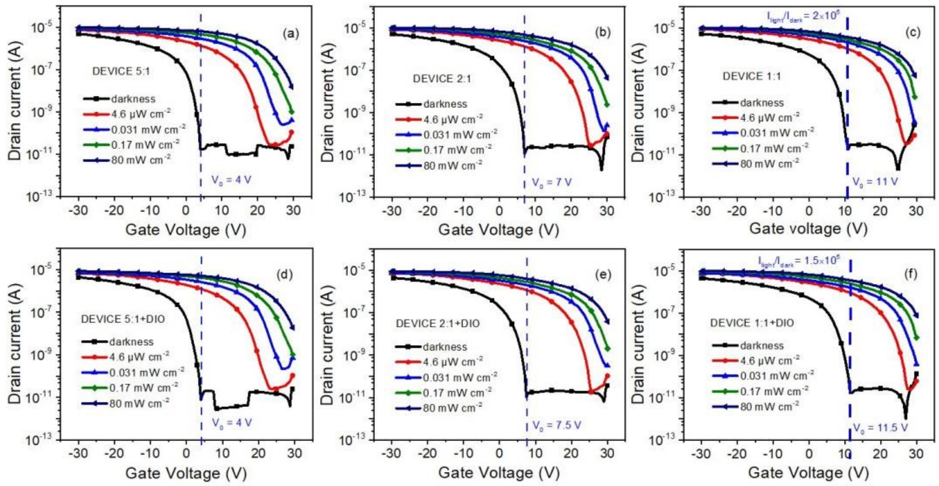

Fig. S8 (a-d) Transfer characteristics curves of OPTs in dark and different light intensity at 820 nm illumination, the drain voltage was set to -60 V.

Table S2 Performance for OPTs (D/A: 1:1) processed w/o and with DIO

	Mobility (cm^2 V^{-1} s^{-1})	Turn-on voltage (V)	I_{light}/I_{dark} ($\times 10^5$)	R ($\times10^3$ A W^{-1})	Gain ($\times10^3$)	τ (ms)	tr (ms)	tf (ms)
w/o DIO	0.26	11	2.0	3.24	4.92	25.1	27.1	113.1
with DIO	0.21	11.5	1.5	2.76	4.19	18.3	15.7	69.6

Concrete parameters of OPTs when the gate voltage was at the corresponding turn-on voltage in devices w/o or with DIO, at -60 V drain voltage under 0.031 mW cm^{-2} illuminations.

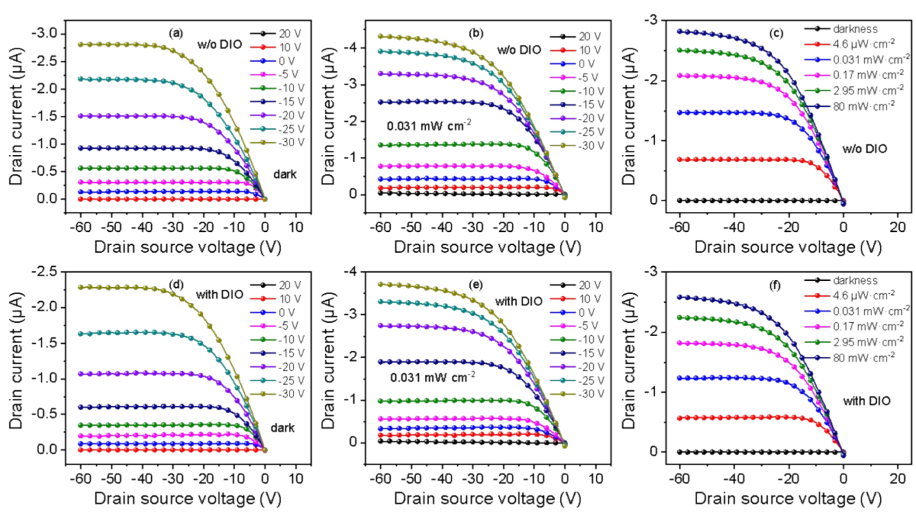

Fig. S9 Output characteristics curves at different gate voltage in dark and 0.031mW cm^{-2} of OPTs (D/A: 1:1) w/o DIO (a, b) and with DIO (d, e), output characteristics curves at different light intensity of OPTs w/o DIO (c) and with DIO (f).

6. Improvement of PSCs photovoltaic results by DIO

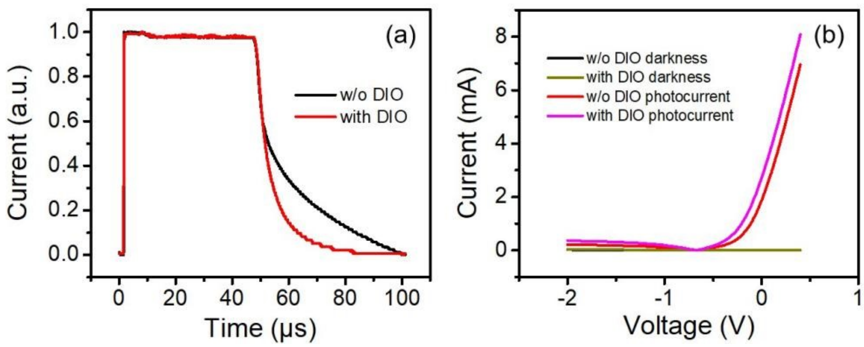

Fig. S10 (a) Time responses under pulsed excitation (0.7 mW cm^{-2} at 820 nm) of the vertical structure w/o DIO and with DIO, (b) I-V curves of the vertical structure w/o and with DIO under dark and an illumination of 100 mW cm^{-2}.

I-V curves of the devices fabricated without/with DIO were plotted in Fig. S10b. A conventional polymer solar cell (PSC) device structure, ITO/ZnO (25 nm)/PDPPBTT:$PC_{61}BM$(D/A 1:1, 85 nm)/MoO_3 (10 nm)/Al (100 nm), was used in this work.

Table S3 Mobility of the devices with the vertical structure w/o DIO and with DIO

	hole mobility ($\times10^{-4}$ cm^2 V^{-1} s^{-1})	electron mobility ($\times10^{-4}$ cm^2 V^{-1} s^{-1})
w/o DIO	1.62	2.52
with 3% DIO	3.42	3.77

Mobility is measured by the space-charge-limited current method, with the device structure: ITO/ZnO/PDPPBTT:$PC_{61}BM$ (without/with 3% DIO)/Al for electron mobility measurement and ITO/PEDOT/PDPPBTT:$PC_{61}BM$ (without/with 3% DIO)/MoO_3/Al for hole mobility measurement.

The phenomenon of current quenching in OPTs with DIO was different from the vertical structure (Fig. S10, after adding DIO, a higher current density). This difference reveals the essential difference in the operating processes of lateral and vertical devices, that the carrier recombination and scattering is more significant in lateral structure with the long carrier channel than that in vertical devices with a short carrier pathway. Especially, the interface between polymer rich phase and $PC_{61}BM$ phase would be enlarged after adding DIO. Thus, the higher quenching efficiency of carriers in diffusion process in DIO devices with interpenetrating network phase lead to a lower mobility than devices without DIO (Table S2), although the light absorption and threshold voltage are similar before and after adding DIO.

7. Semiconductor characteristic parameters of OPTs

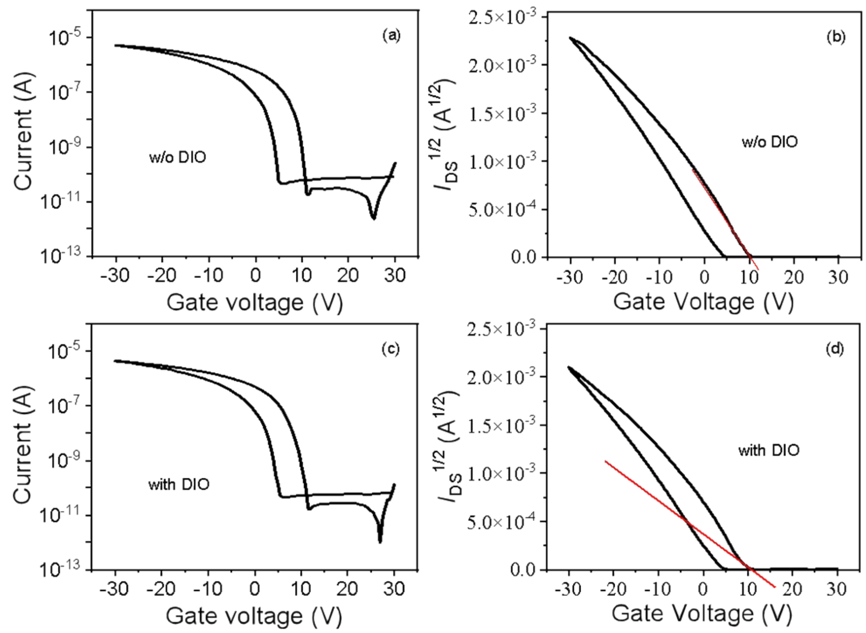

Fig. S11 Transfer characteristics curves of w/o DIO (a, b) and with DIO (c, d), the drain voltages was set to -60 V. (OFET-structure: Si/SiO_2/PMMA (30 nm)/PDPPBTT:PC_{61}BM (D/A: 1:1, 85 nm)/ Au-Au electrodes).

The device mobility (hole saturation mobility in the dark), which is used to characterize semiconductor device features, is calculated according to the following equation:

$$\mu = \frac{2L}{WC_i}\left(\frac{\partial\sqrt{I_{SD}}}{\partial V_G}\right)^2 \tag{S2}$$

Here, *L* is the channel length (40 µm), *W* is the channel width (1000 µm), C_i is the capacitance per unit area of the gate dielectric, I_{SD} is the drain-source current and V_G is the gate voltage.

Table S4 The semiconductor characteristic parameters of OPTs (D/A: 1:1)

	μ (cm^2 V^{-1} s^{-1})	I_{on}/I_{off} (×10^5)	$V_{th-light}$ (V)	$V_{th-dark}$ (V)	ΔV_{th} (V)
w/o DIO	0.26	2	29.5	10.5	19
with DIO	0.21	1.5	30	11	19

8. REFERENCES

1 Y. Fang, J. Huang, *Adv. Mater.,* 2015, **27**, 2804-2810.